FULL PAPER

Open Access

Probabilistic tsunami hazard assessment based on the Gutenberg–Richter law in eastern Shikoku, Nankai subduction zone, Japan

Toshitaka Baba[1*] , Masato Kamiya[2], Naoki Tanaka[2], Yusuke Sumida[2], Ryoichi Yamanaka[3], Kojiro Watanabe[1] and Hiroyuki Fujiwara[4]
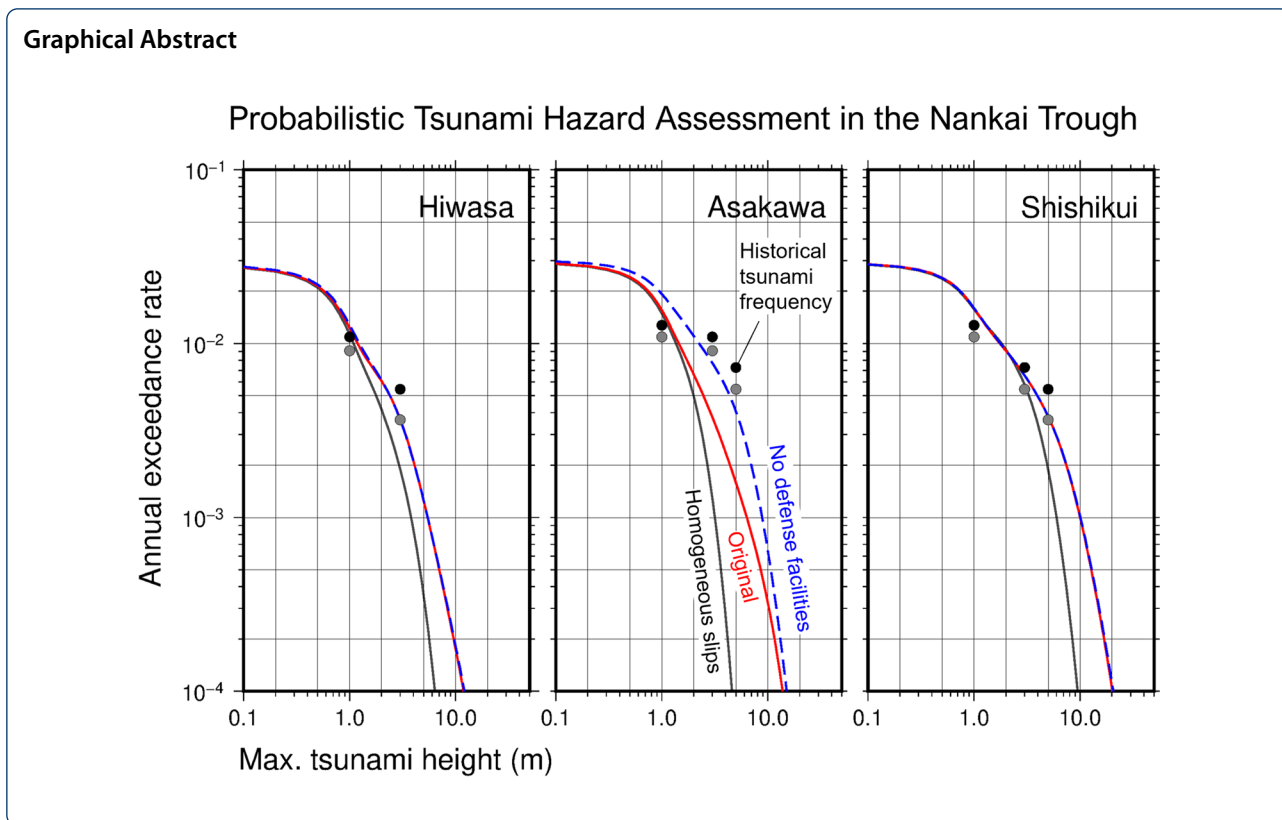
Abstract

Earthquake and tsunami predictions comprise huge uncertainties, thus necessitating probabilistic assessments for the design of defense facilities and urban planning. In recent years, computer development has advanced probabilistic tsunami hazard assessments (PTHAs), where hazard curves show the exceedance probability of the maximum tsunami height. However, owing to the lack of historical and geological tsunami records, this method is generally insufficient for validating the estimated hazard curves. The eastern coast of Shikoku in the Nankai subduction zone, Japan, is suitable for validation because tsunami records from historical Nankai Trough earthquakes are available. This study evaluated PTHAs by comparing the tsunami hazard curves and exceedance frequencies of historical Nankai Trough tsunamis. We considered 3480 earthquake scenarios representing the rupture patterns of past Nankai earthquakes and calculated all tsunamis. The probability of earthquake occurrence was based on the Gutenberg–Richter law. We considered uncertainty in tsunami calculations with astronomical tide variations. The estimated tsunami hazard curves are consistent with the exceedance frequencies obtained from historical tsunamis. In addition, sensitivity tests indicate the significance of the earthquake slip heterogeneity and tsunami defense facilities in PTHAs. We also extended the PTHAs to tsunami inundation maps in high resolution and proposed an effective new method for reducing the tsunami computation load.

Keywords: Probabilistic tsunami hazard assessment, Nankai subduction zone, Gutenberg–Richter law, Historical tsunami

*Correspondence: baba.toshi@tokushima-u.ac.jp

[1] Graduate School of Technology, Industrial and Social Sciences, Tokushima University, Tokushima, Japan
Full list of author information is available at the end of the article

Baba *et al. Earth, Planets and Space*   (2022) 74:156

Page 2 of 17

Graphical Abstract

Probabilistic Tsunami Hazard Assessment in the Nankai Trough

Introduction

The Philippine Sea Plate subducts under the Eurasian Plate at the Nankai Trough (Fig. 1), where great interplate earthquakes are likely to occur. A Japanese government committee developed earthquake source models for the maximum magnitude (M_w 9.1) in the Nankai Trough (Cabinet Office 2012). Local authorities have calculated tsunamis using these source models and constructed deterministic tsunami hazard maps for disaster mitigation (e.g., Tokushima Prefecture 2012). The estimated tsunamis in the deterministic tsunami hazard maps are too high to be stopped using breakwaters owing to construction cost and technological limitations in a number of areas. However, because small and moderate tsunamis occur more frequently than large ones, we must determine the heights and number of seawalls to be built based on benefit–cost analysis. Therefore, probabilistic tsunami hazard assessments (PTHAs) are more useful than deterministic tsunami hazard assessments. While the deterministic tsunami hazard maps encourage residents to evacuate appropriately, PTHAs are valuable for determining hardware logistics, such as the number of seawalls to construct, building disaster-resistant cities, and calculating disaster insurance premiums.

The PTHAs were derived from probabilistic seismic hazard assessments (Cornell 1968; SSHAC 1997; Toro et al. 1997; Anderson and Brune 1999). Past studies on PTHAs (Geist 2002; Geist and Parsons 2006; Annaka et al. 2007) divided the uncertainties of tsunami hazards into epistemic and aleatory uncertainties. They used logic trees to capture the epistemic uncertainty and assumed probabilistic density functions in tsunami water levels to evaluate aleatory uncertainty. Because tsunamis are sensitive to heterogeneous fault slip motions, several studies have proposed methods for constructing multiple heterogeneous fault slip models stochastically (Goda et al. 2014; Mueller et al. 2015; Davies et al. 2015; Melgar et al. 2016). Goda et al. (2014) applied spectral analysis in the extraction of the spatial correlation characteristics of slip patterns using inversion slip models of past megathrust earthquakes. They then randomly varied the spectral phase to generate a number of heterogeneous slip models while retaining the slip characteristics. Recent PTHAs have accounted for many heterogeneous slip models generated via such methods (Fukutani et al. 2015; LeVeque et al. 2016; Sepúlveda et al. 2017; Crempien et al. 2020; Fujiwara et al. 2020). Fujiwara et al. (2020) defined seismic segments based on past interplate earthquakes along the Nankai Trough off southwestern Japan and constructed systematic heterogeneous slip models for PTHAs along the coast of southwestern Japan.
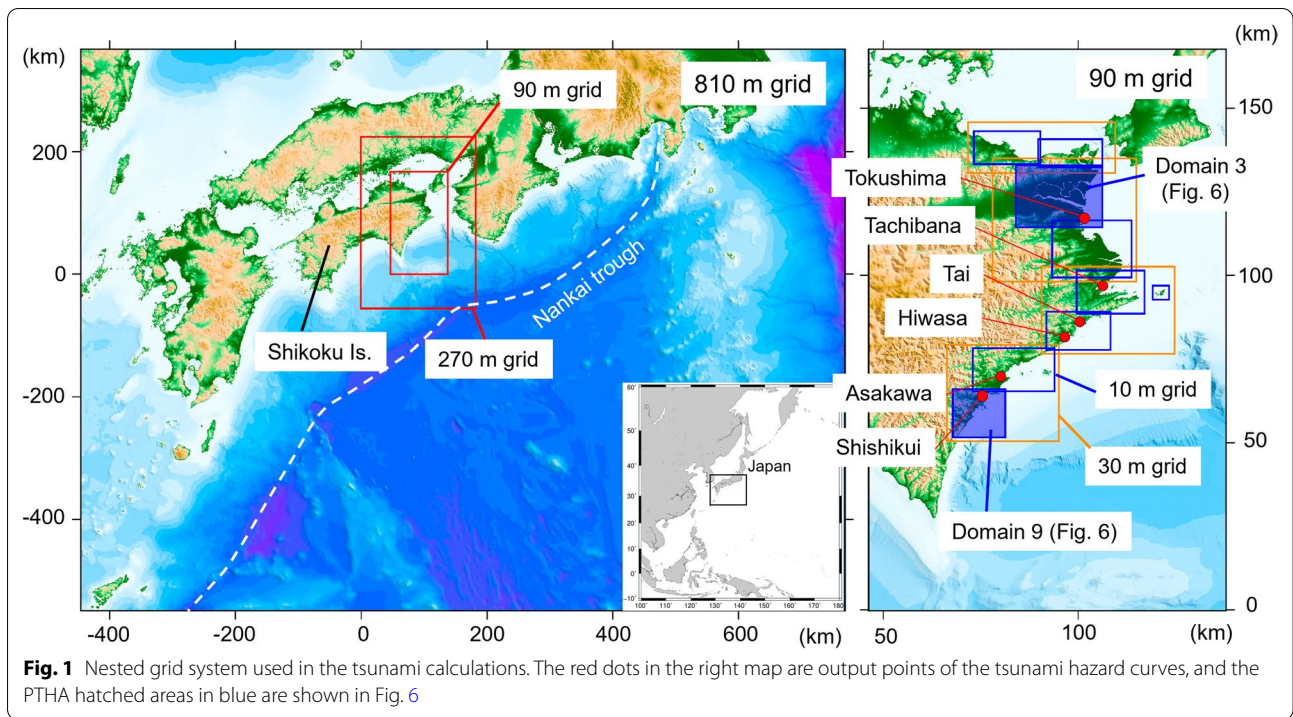
Baba *et al. Earth, Planets and Space* (2022) 74:156

Page 3 of 17

Fig. 1 Nested grid system used in the tsunami calculations. The red dots in the right map are output points of the tsunami hazard curves, and the PTHA hatched areas in blue are shown in Fig. 6

Many heterogeneous slip models require huge effort in tsunami computations; therefore, methods for reducing the computational load have been actively discussed in numerous studies, for example, Løvholt et al. (2012, 2015), Lorito et al. (2015), Glimsdal et al. (2019), Volpe et al. (2019), Kotani et al. (2020), and Fukutani et al. (2021). Løvholt et al. (2012, 2015) numerically calculated offshore tsunamis only and then applied amplification factors to estimate the maximum tsunami inundation heights. However, because this method is less accurate at inland locations, Lorito et al. (2015) and Volpe et al. (2019) estimated the tsunami height distribution along the contours with a water depth of 50 m in the first coarse calculations. They eliminated similar scenarios of tsunami height distributions in the second high-resolution tsunami inundation calculations and obtained PTHA maps for inundation depths. Fukutani et al. (2021) applied a singular value decomposition method to a small number of inundation depth distributions to extract their characteristic modes. Linear summations of the high-impact modes can randomly generate many surrogate inundation depth distributions by changing the weight among the modes.

Behrens et al. (2021) summarized the methods and challenges associated with current PTHAs. One of the most critical challenges is the lack of long-term observational data. While we want to validate PTHAs for tens of thousands of years, instrumental observations of earthquakes and tsunamis have only been available for approximately 100 years. To the best of our knowledge, Geist and Parsons (2006) performed the only comparison of estimated tsunami hazard curves with observations recorded at tide gauges in the past 100 years. This type of verification is generally insufficient for PTHAs. However, the Nankai Trough is an appropriate region for validating PTHAs, where historical tsunami records are relatively available. In this study, we compare the probabilistic tsunami hazard curves with historical tsunami data from the Nankai Trough to evaluate the accuracy of PTHAs.

The remainder of the manuscript is structured as follows. "Heterogeneous slip models for interplate earthquakes in the Nankai Trough" describes the 3480 cases of heterogeneous earthquake slip models used in this study (Fujiwara et al. 2020). "Methods for probabilistic assessments" explains the method of PTHAs, including high-resolution tsunami inundation calculations on a high-performance computer. "Sensitivity test settings" explains the settings used for the sensitivity tests. "Probabilistic tsunami hazard assessment results" presents the results of the PTHAs, and "Discussion" compares the tsunami hazard curves with the historical tsunami exceedance frequency. In addition, we propose an efficient method for reducing the calculation load for creating tsunami inundation probability maps. We illustrate an application of tsunami inundation probability maps as a practical problem for tsunami-resilient communities.

Baba *et al. Earth, Planets and Space*   (2022) 74:156

Page 4 of 17

Heterogeneous slip models for interplate earthquakes in the Nankai Trough

Fujiwara et al. (2020) divided the Nankai Trough subduction zone into 18 seismic segments, 6 in the direction of the trough axis (A to E and Z) and 3 in the direction of plate subduction (shallow, middle, and deep). They combined these segments to define 83 different earthquake source regions by considering the rupture patterns of past Nankai Trough earthquakes combined with seismic and geophysical observations. The event magnitudes in the source region range from M_w 7.6 to M_w 9.1, according to an earthquake scaling law. Each source region has multiple heterogeneous slip models, where a large slip patch and super-large slip patch exist in the background slip area corresponding to the extent of the source region.

Upon generating the heterogeneous slip models, the large slip patch systematically shifts by a half of the patch area in the direction of the fault strike and dip in the source region. However, the deep segment may not solely exhibit significant slip because it overlaps with the deep low-frequency earthquakes and slow-slip regions (e.g., Obara 2002; Obara et al. 2004; Obara and Kato 2016). Therefore, Fujiwara et al. (2020) did not create models with large slips occurring only in the deep segment. The number of large slip patches was set to one for small source regions and 1 or 2 for large ones. When a fault rupture reaches the trench axis, an extremely large slip may occur, generating a giant tsunami (e.g., Satake et al. 2013). To consider the influence of such slip on tsunami generation, Fujiwara et al. (2020) developed models where a super-large slip patch lies in a large slip patch near the trough axis. The super-large slip patch was located at the center of the large slip patch in the fault strike direction. In the fault dip direction, the upper edge of the super-large slip patch was tangential to the trough axis. The slip amounts of the large and super-large slip patches were twice and four times larger than that of the background slip area, respectively. The area of the source region determines the magnitude, and the slip amount was adjusted accordingly. The area ratios of the large and super-large slip patches were 30% and 10% of the total area of the source region, respectively. For the shape of the large and super-large slip patches, the ratio of the length and width of the patches was set to 2:1.

Fujiwara et al. (2020) used this method to propose 3480 models of heterogeneous earthquake slip occurring in the Nankai Trough subduction zone (Additional file 1: Fig. S1). Although this method requires a manual setup rather than automatic generation methods such as those reported by Goda et al. (2014) and Mueller et al. (2015), this dataset can best explain the various occurrence patterns of the interplate earthquakes in the Nankai Trough with a relatively small number of scenarios.

Methods for probabilistic assessments
Overall procedure

The overall PTHA procedure used in this study was as follows (Additional file 1: Fig. S2), and the details of the methodology are presented in "Tsunami calculations, Earthquake occurrence probability based on the Gutenberg-Richter law", "Modeling uncertainty and astronomical tide variation", "Tsunami hazard curves and inundation probabilities". We calculated the tsunamis from all 3480 heterogeneous slip models proposed by Fujiwara et al. (2020). We assumed that the calculated tsunami water levels contain modeling errors in the form of a lognormal distribution function, following previous studies (e.g., Fujiwara et al. 2020; Mulia et al. 2020). Epistemic uncertainty, such as the occurrence probability of an earthquake scenario, was defined using the Gutenberg–Richter (G-R) law (Gutenberg and Richter 1941). As we assessed the probability of tsunami inundation depth distributions, we needed to consider the variation in astronomical tide levels. Therefore, the probability density distribution of the astronomical tide level in the target area was downloaded from the JMA website (see Availability of data and materials) and convolved with the calculated tsunami water level including uncertainty. We provided the PTHAs in the form of tsunami hazard curves near the coast (red dots in Fig. 1) and tsunami inundation depths (blue boxes in Fig. 1).

Tsunami calculations

We solved the nonlinear long-wave equations using the staggered-grid leapfrog difference method with a nested algorithm for 3480 tsunami calculations. In concrete terms, we used the open-source tsunami software JAGURS (Baba et al. 2015, 2017). High-resolution topographic/bathymetric data and bottom friction coefficients (Manning's roughness coefficients) required for the tsunami calculations were the same as those used in deterministic tsunami hazard maps from the local government in Tokushima Prefecture (2012). A nesting gridding system efficiently improved the topographic resolution (Fig. 1), resulting in a minimum spatial resolution of 10 m in the coastal area of eastern Shikoku. The heights of the topographic and the tsunami defense facility data were reduced by 1.0 m, assuming the astronomical tide level was 1.0 m in the calculations. The tsunami inundation varied depending on the tide level when the tsunami occurred. As discussed in "Modeling uncertainty and astronomical tide variation" we considered the probability density distribution of the astronomical tide variation in the uncertainty. Still, this method cannot represent the variation in the horizontal position of the tsunami inundation limit. Therefore, we assumed a high tide status to be a severe case by reducing the height of the topographic and defense facility data. The 3480

Baba *et al. Earth, Planets and Space*   (2022) 74:156

Page 5 of 17

heterogeneous slip models reported by Fujiwara et al. (2020) calculated seafloor crustal movements using the analytical solution obtained by Okada (1985) for a semi-infinite homogeneous elastic body. In addition to the vertical component of the crustal movement, estimations of the tsunami initial water level considered the tsunami excitation due to horizontal movement of the seafloor slope using the equation reported by Tanioka and Satake (1996) and the hydraulic filter proposed by Kajiura (1963). The rise time of the sea surface was 60 s. The topographic data were modified simultaneously following the vertical crustal displacement in the calculations, indicating that it considered the uplift and subsidence of the land due to the fault movements. A tsunami calculation time of 6 h encompassed the maximum wave arrivals in all evaluation areas. The numerical time step was set to 0.1 s to satisfy the stability condition. We used high-performance computers for the 3480 calculations.

This topographic/bathymetric dataset provided tsunami defense facilities, such as tsunami breakwaters, seawalls and river levees, with finite heights in different input files. In our calculations, the tsunami defense facilities were regarded as reflective boundaries when the water level in front of the facilities was lower than the top height, and after the water level exceeded the top height, the defense facilities were eliminated from the calculations assuming the facilities had been completely collapsed by overflow. However, in reality, because overflowing water would not immediately destroy a defense facility, the calculated probability of tsunami inundation may be slightly larger than the actual one. Unfortunately, the accurate modeling of the destruction of a defense facility based on our current knowledge is complicated. Conversely, considering the safety factor in practical hazard predictions is typical, making our considerations in the tsunami calculations suitable for disaster mitigation purposes.

Earthquake occurrence probability based on the Gutenberg–Richter law

Fujiwara et al. (2020) used the probability of Nankai Trough earthquakes for the subsequent 30 years estimated by Headquarters for Earthquake Research Promotion (2013) that assumed an update process following the Brownian passage time distribution. They used logic trees to determine the weight of the Nankai earthquake occurrence patterns. Because this study focused on comparing PTHAs with the exceedance frequency from historical tsunami data, we needed to acquire PTHAs for an extended period. Therefore, we assumed the stationary Poisson distribution and applied the G-R law using the Japan Meteorological Agency (JMA) earthquake catalog

(see Availability of data and materials) to determine the earthquake occurrence probability ($P(E_i)$), which presents a major methodological difference from that of Fujiwara et al. (2020). The catalog period ranged from 1919 to 2019. We selected earthquake data with the following criteria: a magnitude of ≥ 5, a depth of ≤ 50 km, and beneath the sea from 131°E to 139°E and 30°N to 36°N surrounding the Nankai Trough subduction zone. Both the 3480 earthquake scenarios and historical tsunami data were used for the interplate earthquakes. However, the earthquake catalog contains all types of earthquakes. We used the earthquake focal mechanism solution data available after October 1997 to focus on the frequency of reverse fault-type earthquakes. The post-October 1997 catalog determined the focal mechanisms of 63 earthquakes, and 35 of 63 indicated dip-slips on reverse faults. We multiplied 35/63 by the number of earthquakes in the JMA catalog and divided them by the period of 101 years to obtain the annual frequency of reverse fault earthquakes in the target region. Finally, we obtained the following G-R law equation:

$$log_{10}(n_M) = 2.935 - 0.687M \pm 0.155, \qquad (1)$$

where n_M is the annual frequency of reverse fault-type earthquakes of magnitude M. The width of the magnitude bin was set to 0.1 to estimate the equation. The error indicates that the standard deviation refers to $log_{10}(n_M)$. The sensitivities of the parameters of the G-R equation to the tsunami exceedance rate are discussed in "Sensitivity test settings" and "Probabilistic tsunami hazard assessment results".

We compared the G–R equation to the moment rate accumulated at the plate boundary in the Nankai Trough. Assuming the seismic coupling zone to be 700 km long and 200 km wide, a plate convergence rate of 4 cm/year, and rigidity of 50 GPa, the moment accumulation rate was calculated to be 2.8×10^{20} Nm/year. The moment release rate predicted from the G–R equation (Eq. 1) was approximately 1.6×10^{20} Nm/year. This value was reasonable because the assumed coupled zone (700×200 km^2) included the deep seismic segments where deep low-frequency earthquakes and slow slips occurred.

The occurrence probability for each heterogeneous slip model ($P(E_i)$) follows a tree structure (Additional file 1: Fig. S3). The G-R law in Eq. (1) defines the annual occurrence frequency of each magnitude in the Nankai Trough. Because each magnitude has multiple source regions, we distributed the value of the annual frequency equally to each region. In addition, because each source region has multiple heterogeneous slip models, the annual frequency assigned to the source region was further divided equally among these models.

Baba *et al. Earth, Planets and Space* (2022) 74:156

Page 6 of 17

Modeling uncertainty and astronomical tide variation

PTHAs consider the uncertainties in the calculated tsunami height. We assumed that the true value of the tsunami height exists in a probability density distribution around the calculated value. Fujiwara et al. (2020) and Mulia et al. (2020) approximated the probability density function $f(x)$ of the tsunami height using a lognormal distribution with the calculated value as the median, as shown in the following equation:

$$f(x) = \frac{1}{\sqrt{2\pi}\sigma x}\exp\left\{-\frac{(\ln x - \lambda)^2}{2\sigma^2}\right\}, \quad (2)$$

where λ is the natural logarithm of the calculated tsunami height, and σ is the natural logarithm of the standard deviation of the calculated tsunami height.

In determining σ, the following uncertainties must be considered in the calculated tsunami height: (a) the analytical approximation error using the nonlinear long-wave equations; (b) the discretization error due to the discretization of the governing equations for the numerical calculations; (c) the error due to the representation of complex fault motion by a simplified source fault model; (d) the error included in the crustal movement calculation due to the replacement of the actual earth by a semi-infinite homogeneous medium; (f) the accuracy of the bathymetry and elevation data used to create the topographic model; and (g) the discretization error of the topographic model in the numerical calculations. However, investigating each factor of uncertainty in the estimation of tsunami height causes is complicated. Therefore, we did not evaluate each uncertainty, but assumed that the error between the observed and calculated values for the actual tsunamis could represent the total uncertainty from (a) to (g). In the reproducibility study performed by Fujiwara et al. (2020) using tsunami inundation traces from the 2011 off the Pacific coast of Tohoku Earthquake, the variation index of Aida (1978) ($\kappa = 1.42$; $\sigma = \ln(\kappa) = 0.35$) was found to be reasonable. We used their method and σ values in the present study. Kitou et al. (2021) evaluated how well the heterogeneous source models can simulate the tsunami trace heights of the 1944 Tonankai and 1946 Nankai earthquakes, the most recent interplate earthquakes in the previous earthquake cycle. The model that reproduced the tsunami trace heights indicated $\kappa = 1.35$ for the 1944 Tonankai earthquake and $\kappa = 1.49$ for the 1946 Nankai earthquake. Therefore, the value of $\kappa = 1.42$ adopted in this study is reasonable for Nankai Trough earthquakes.

Because Eq. 2 is a long tail function, we must define a truncated range for integration to obtain a cumulative probability function. Fujiwara et al. (2020) examined the distribution of tsunami trace height ratio data, computed ratios of the 2011 Tohoku earthquake, and found that the data range was approximately $\pm 3\sigma$. In this study, we used $\pm 3\sigma$ as the truncated range of integration.

The height of the astronomical tide level during a tsunami attack impacts the tsunami inundation depths on land. We incorporated the effects of astronomical tide levels in PTHAs using the method described by Thio and Li (2015). They expressed the tide level using a probability density function following an emergence frequency and convolved it with the tsunami height probability density function (Eq. 2). We used the tide tables for 2021 on the JMA website (see Availability of data and materials) to estimate the frequency distributions of the astronomical tide levels in the target regions.

The maximum tsunami inundation area should appear at the highest tide level with the maximum tsunami scenario in the database. However, the tide level convolution method applied in this study does not change the horizontal location of the inundation limit of the inland tsunami following the tide levels. Therefore, we performed the tsunami calculations at the maximum tide level of $+1.0$ m and convolved the tide probability function downward. Using the probability density functions after the convolution with the tide, we calculated the probability that the highest tsunami water level, H, exceeds a designated height, h, for each heterogeneous slip model ($P(H > h|E_i)$).

Tsunami hazard curves and inundation probabilities

The annual rate of the highest tsunami water level H exceeding a designated height h at a hazard assessment point ($P(H > h)$) is expressed by the following equation, assuming the stationary Poisson distribution and that the heterogeneous slip models are probabilistically independent:

$$P(H > h) = 1 - \prod_{i=1}^{3480}\left\{1 - P(E_i)P(H > h|E_i)\right\}. \quad (3)$$

The 6 output points of the hazard curves are presented in red in Figs. 1, 2. For the inundation depth, we converted the tsunami height to the inundation depth measured from the topographic surface after the crustal movement and then constructed the hazard curves on the land area using Eq. (3). All inundation points on land estimated the frequency of the annual inundation depth exceedances of 0.3 m, where a tsunami drifts a person, and of 2.0 m, where a tsunami causes wooden houses to collapse (Shuto 1993; Koshimura et al. 2009).
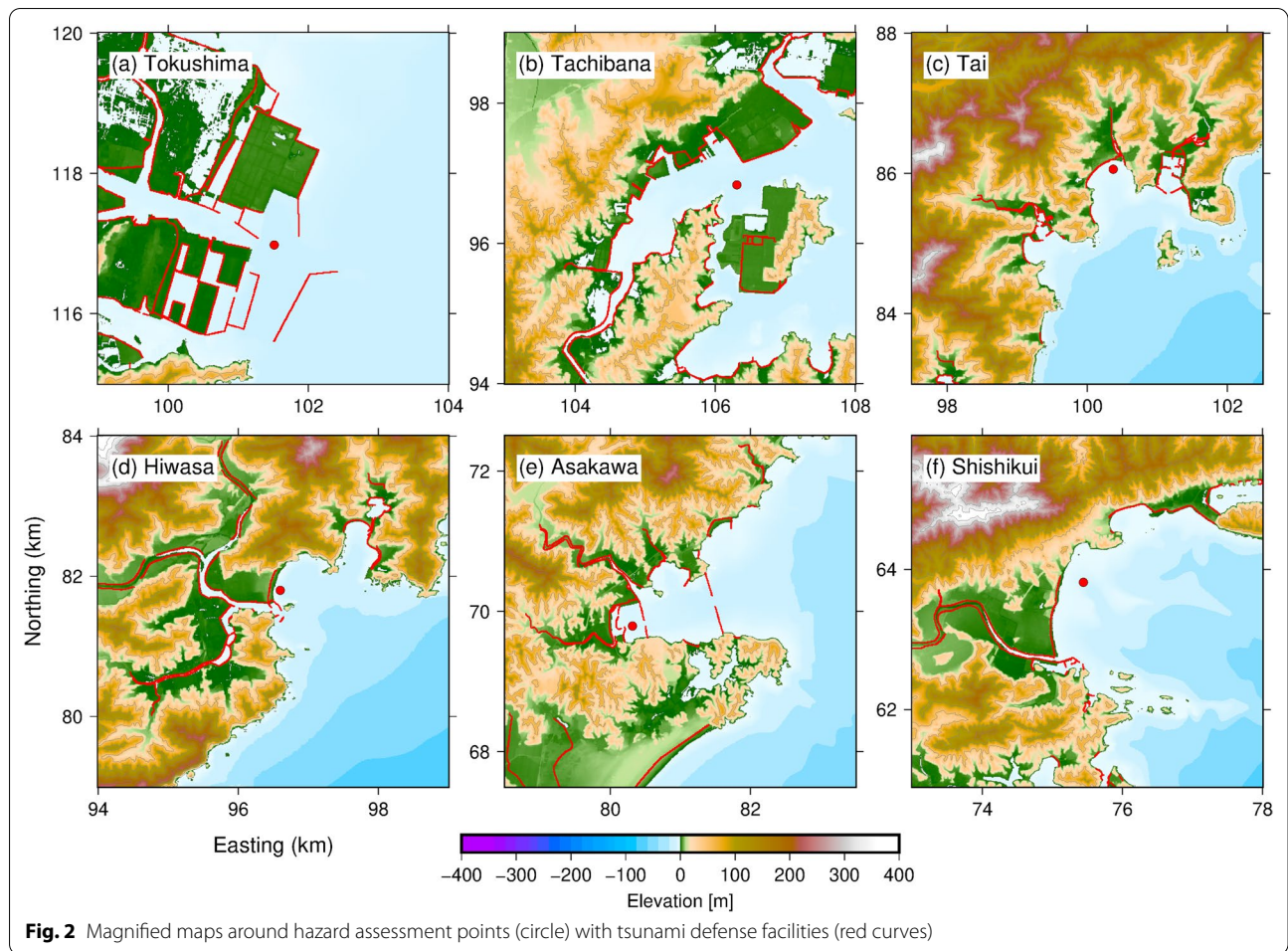
Fig. 2 Magnified maps around hazard assessment points (circle) with tsunami defense facilities (red curves)

Table 1 Gutenberg–Richter (G–R) equations ($\log_{10}(n_M) = a - bM \pm c$) used for the sensitivity tests

	a	*b*	*c*	Earthquake data used to construct G-R equation
A	2.935	0.687	0	$M > 5.0$, since 1919, depth < 50 km, earthquakes in ocean region, dip-slip reverse fault type (original)
B	2.935	0.687	+0.155	Same as A, but shifted by standard deviation
C	2.935	0.687	−0.155	Same as A, but shifted by standard deviation
D	2.764	0.658	0	The condition of $M > 2$ differs from A
E	0.344	0.379	0	The condition of since 1997 differs from A
F	3.645	0.766	0	The condition of all depths differs from A
G	3.623	0.766	0	The condition of earthquakes in terrestrial and ocean regions differs from A
H	3.204	0.687	0	The condition of all slip types differs from A

Sensitivity test settings

There are two primary sources of error in the procedure used to estimate tsunami hazard curves in this study: the accuracy of the tsunami calculation and the earthquake occurrence probability parameters. The uncertainty considers the tsunami calculation error using the lognormal function with a standard deviation σ (Eq. 2). We regarded 0.35 as the most plausible value for σ, which corresponds to $\kappa = 1.42$ and is based on the comparisons between the calculated and observed values of the past tsunami events. However, determining σ is debatable. Therefore, we conducted a sensitivity analysis by changing the value of σ.

Baba *et al. Earth, Planets and Space*   (2022) 74:156

Page 8 of 17

We required the G-R equation to determine a seismicity rate averaged over an extended period of time, as a comparison with historical tsunamis was an objective of this study. Unfortunately, existing seismic catalogs include data from the last 100 years, and it is impossible to estimate the G-R equation for a period exceeding 100 years. Seismic activity may have fluctuated over a period exceeding 100 years. Even within the last 100 years, earthquake detection capacity was not constant owing to the development of a seismic observation network. The estimation of these uncertainties in the G-R equation is challenging. Therefore, we conducted an additional sensitivity analysis of the G-R equation to investigate its effect on the tsunami hazard curves. Table 1 summarizes the cases that were investigated in the sensitivity analysis. Case A was the G-R equation used to create the original hazard curves. Cases B and C shifted the G-R equation from case A by one standard deviation (± 0.155). Case D changed the lower magnitude limit for estimating the G-R equation from 5.0 to 2.0. Case G used earthquakes located in terrestrial and ocean regions. Case H utilized all earthquake types instead of only using dip-slip reverse fault events. Case H provided the highest earthquake rate of the cases, corresponding to the moment release rate of 3.0×10^{20} Nm/year. This rate was almost identical to the rough estimation of the moment accumulation rate (2.8×10^{20} Nm/year) in the Nankai Trough.

We used the heterogeneous slip models of 3480 cases in the Nankai Trough for tsunami evaluation. In contrast, examining the change mechanism of the hazard curves changes using homogeneous slip models would be interesting. Therefore, we created the homogeneous slip models in this test. Although multiple heterogeneous slip models were defined for each earthquake source region, the homogeneous slip generates one slip model per source region. The total number of homogeneous slip models was 83 cases, which was the same as that of the source regions. The tsunami calculations were then performed again to create a tsunami database for the homogeneous slip models.

In Asakawa Bay (Fig. 2e), where tsunami disasters have occurred repeatedly, the residents constructed two large tsunami breakwaters at the bay mouth and inside the bay following the last Nankai earthquake in 1946. The original tsunami hazard curves included the effects of tsunami breakwaters as linear structures in the tsunami calculations. The location where tsunami hazard curve estimated for Asakawa Bay was behind these breakwaters. Breakwaters also existed on the seaward side of the output point of the tsunami hazard curve in Tokushima (Fig. 2a). The other hazard assessment areas had seawalls along the coastline and levees along rivers, but no offshore breakwaters. We performed the tsunami calculations for all 3480 cases excluding the tsunami defense facilities (i.e., red curves in Fig. 2) and then compared the estimated tsunami hazard curve with the original curve to investigate whether the tsunami mitigation effect was presented in the hazard curves.

Probabilistic tsunami hazard assessment results

The red curves shown in Fig. 3 are the tsunami hazard curves obtained in this study. The annual exceedance rate ranges from 6.6×10^{-3} to 1.8×10^{-2} times/year for the maximum water level of 1 m, 6.6×10^{-4} to 6.8×10^{-3} times/year for 3 m, 5.8×10^{-5} to 4.0×10^{-3} times/year for 5 m, and 1.8×10^{-7} to 1.0×10^{-3} time/year for 10 m along the eastern coast of Shikoku. The recurrence interval is approximated to be the reciprocal of the annual exceedance rate. The maximum tsunami water levels for the 100-, 1000-, and 10,000-year recurrence intervals are 0.8–1.9, 2.7–10.2, and 4.5–20.4 m, respectively. The probability increases close to the source region of the Nankai earthquakes. As the recurrence interval increases, the tsunami height increases.

Figure 3 shows the tsunami hazard curves estimated using $\sigma = 0.05$, 0.20, 0.50, 0.65, 0.80, and 0.95 (corresponding to $\kappa = 1.05$, 1.22, 1.65, 1.92, 2.23, and 2.59, respectively). The annual exceedance rate increased as the value of σ increased. The difference in the exceedance rate was significant at large tsunami heights, indicating the significance of the σ value in PTHAs.

Curves B and C in Fig. 4 show the variations corresponding to the standard deviation error in the G-R law equation, where the annual exceedance rate varied by $\pm 40\%$. The hazard curves for the other cases fell within the 1σ error range between curves B and C, except for curve H, where all earthquake types were utilized, not solely dip-slip reverse fault events. Compared with the results of the σ sensitivity study, the variations in the exceedance rate were relatively low for significantly high tsunamis. However, this does not mean that there is no effect on the large tsunami heights, as Fig. 4 uses a double-logarithmic scale. Differences in both large and small tsunami heights were observed equally.

The tsunami hazard curves estimated using the homogeneous slip models were clearly lower than the original curves (Fig. 5), indicating the need to incorporate earthquake slip heterogeneity of earthquakes in PTHAs. In Asakawa Bay, tsunami disaster mitigation using tsunami breakwaters was observed in the hazard curve, indicating that PTHAs can aid in the design of tsunami protection facilities.

Figure 6a, c shows the distributions of the annual exceedance rate for tsunami inundation depths in
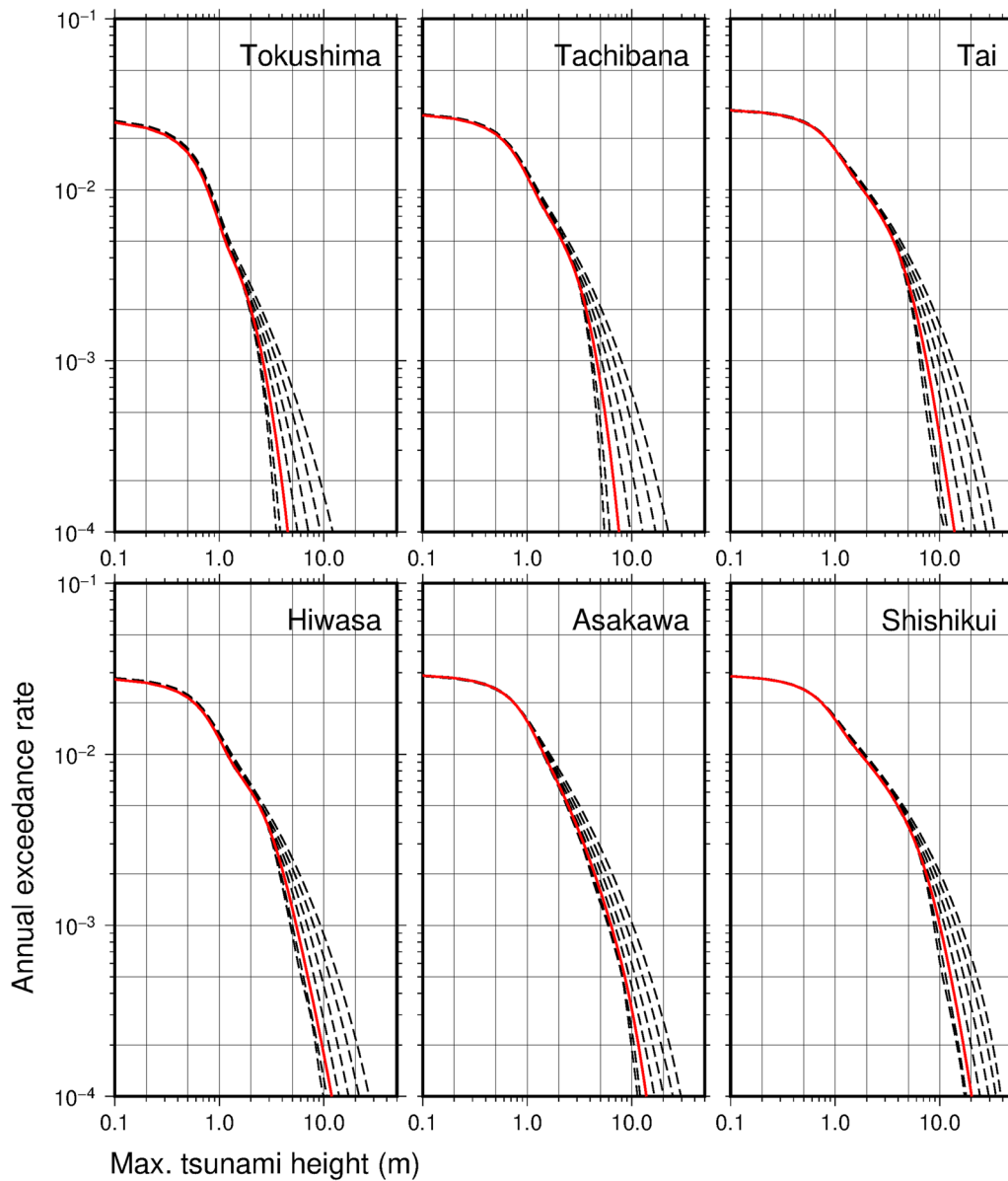
Baba *et al. Earth, Planets and Space*   (2022) 74:156

Page 9 of 17

Fig. 3 Tsunami hazard curves for a variable σ (Eq. 2) at 6 sites (shown in Fig. 1). The original curves are presented in red ($\sigma = 0.35$). The dashed curves were obtained using $\sigma = 0.05, 0.20, 0.50, 0.65, 0.80,$ and 0.95, respectively, from the smallest to largest probability

domains 3 and 9, respectively. Domain 3 has a large inundation area because of the low elevation land in the river delta. The maximum annual rate of exceedance for an inundation depth of 0.3 m or greater is approximately 6.0×10^{-3} times/year. In this area, tsunamis enter rivers and overflow from locations where river levees are relatively low; therefore, the probability is not necessarily higher along the coast near the sea. The maximum annual rate exceedance of 2.0 m (Additional file 1: Fig. S4) is approximately 2.5×10^{-3} times/year, which

is approximately 40% of the exceedance rate of that for 0.3 m inundation depth.

Domain 9 has a ria topography. The annual exceedance rate is high along the coast, and the probability value decreases with distance from the coast (Fig. 6c). The maximum annual exceedance rate for a depth of 0.3 m is approximately 2.5×10^{-2} times/year, and that for a depth of 2.0 m is approximately 1.0×10^{-2} times/year. These values are approximately 400% of those in domain 3.
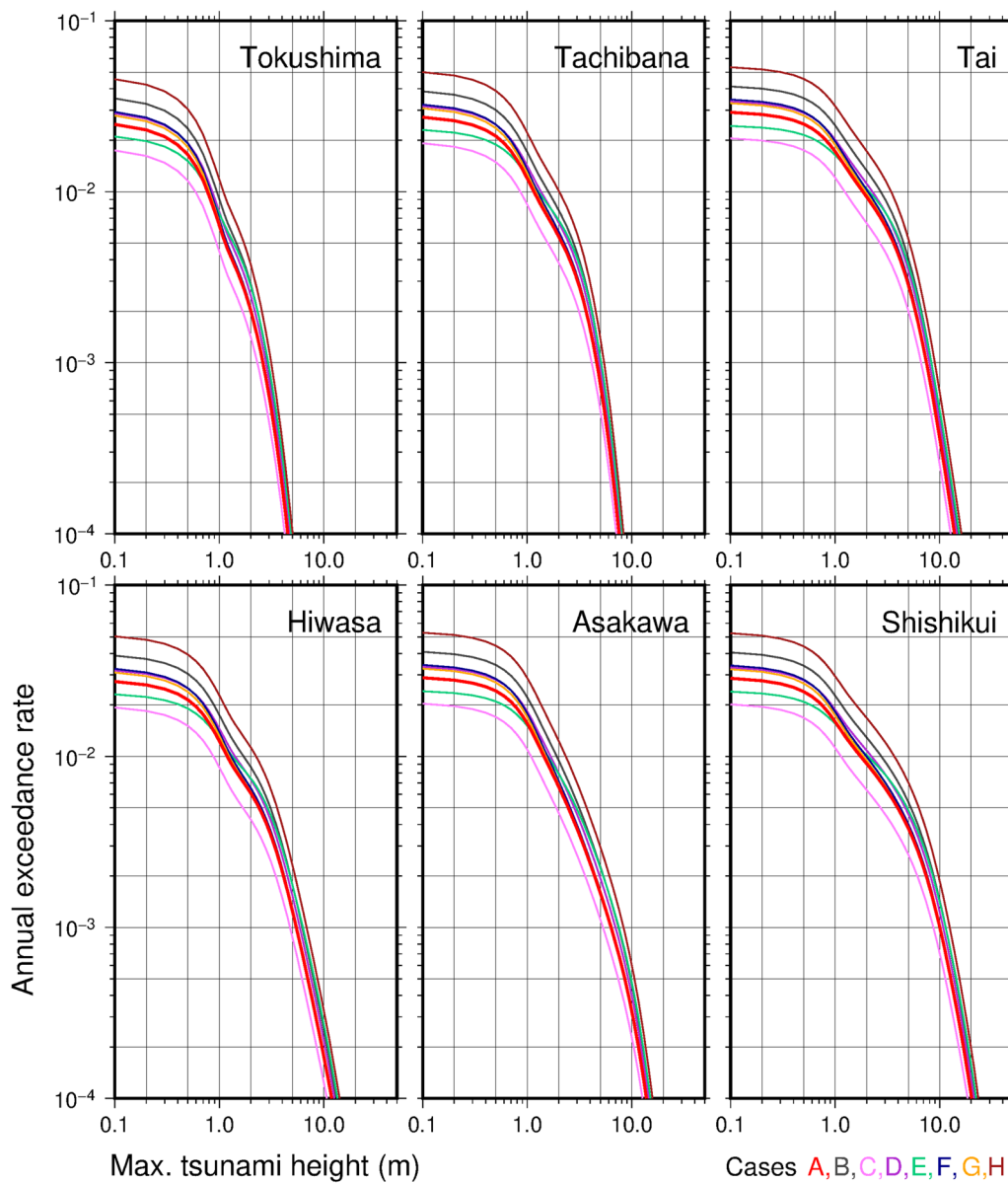
Fig. 4 Tsunami hazard curves for variable Gutenberg–Richter (G-R) equations at 6 sites (Fig. 1). Please see Table 1 for the G-R equations of cases A–H

Discussion

Comparison with historical tsunami data

Multiple records of past tsunamis should be acquired to validate the obtained PTHA results. However, because the recurrence period of large tsunamis is long, such long-period data are non-existent. Therefore, the validity of the obtained hazard curves comparing the actual observational data has not been significantly evaluated in previous studies. Our target area, the Nankai Trough, is a desirable region in this sense because the repetition of interplate earthquakes is well documented

(Ishibashi 2004), and there are numerous records of tsunami heights hitting the coasts (e.g., Hatori 1978, 1981, 1988; Murakami et al. 1996; Tohoku University and JNES last access in 2021). These historical tsunami data have been used to construct several earthquake fault models for past earthquakes (e.g., Annaka et al. 2003; Furumura et al. 2011). This section calculates the annual exceedance rate using historical tsunami data and fault models and compares it with the tsunami hazard curves.

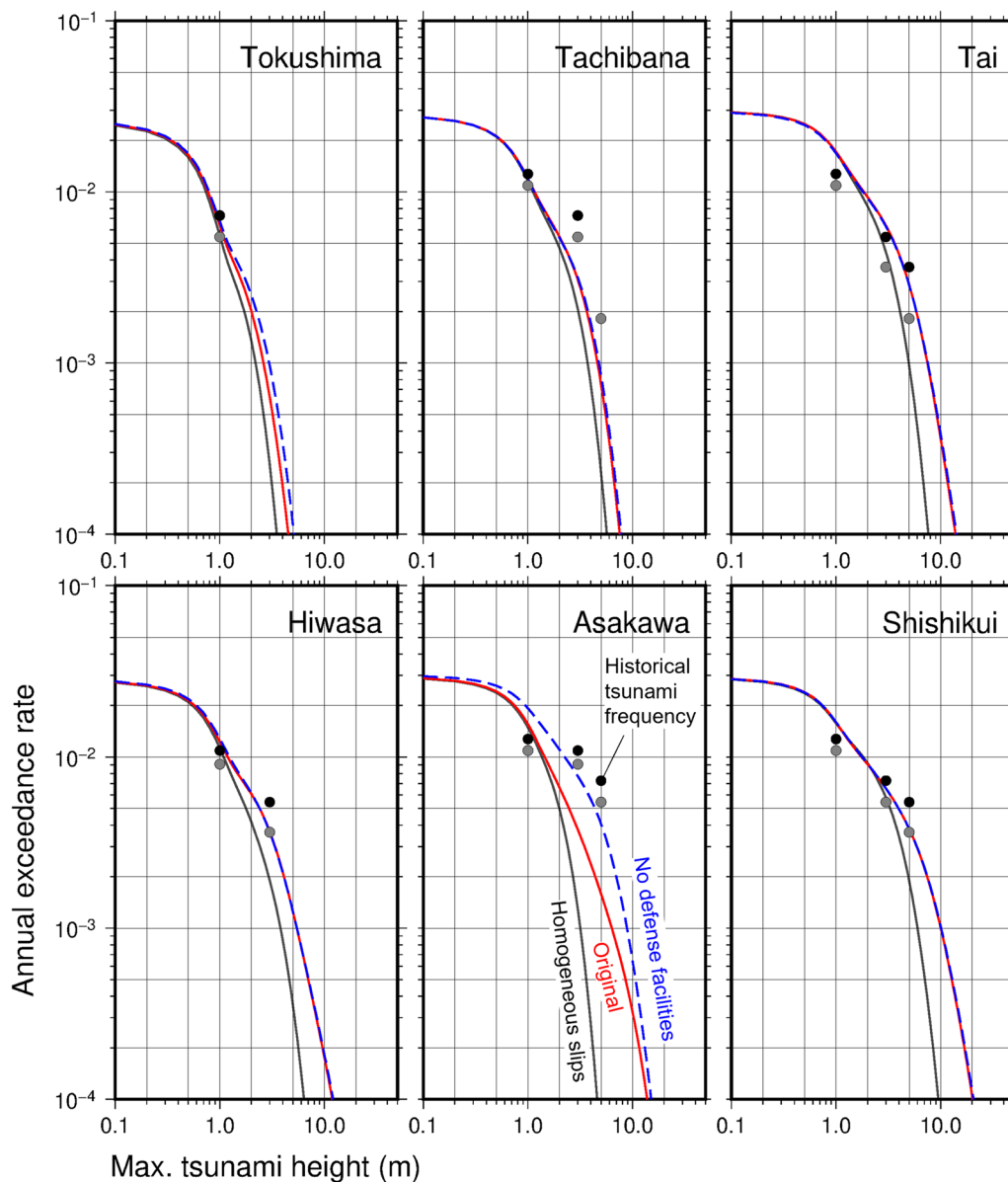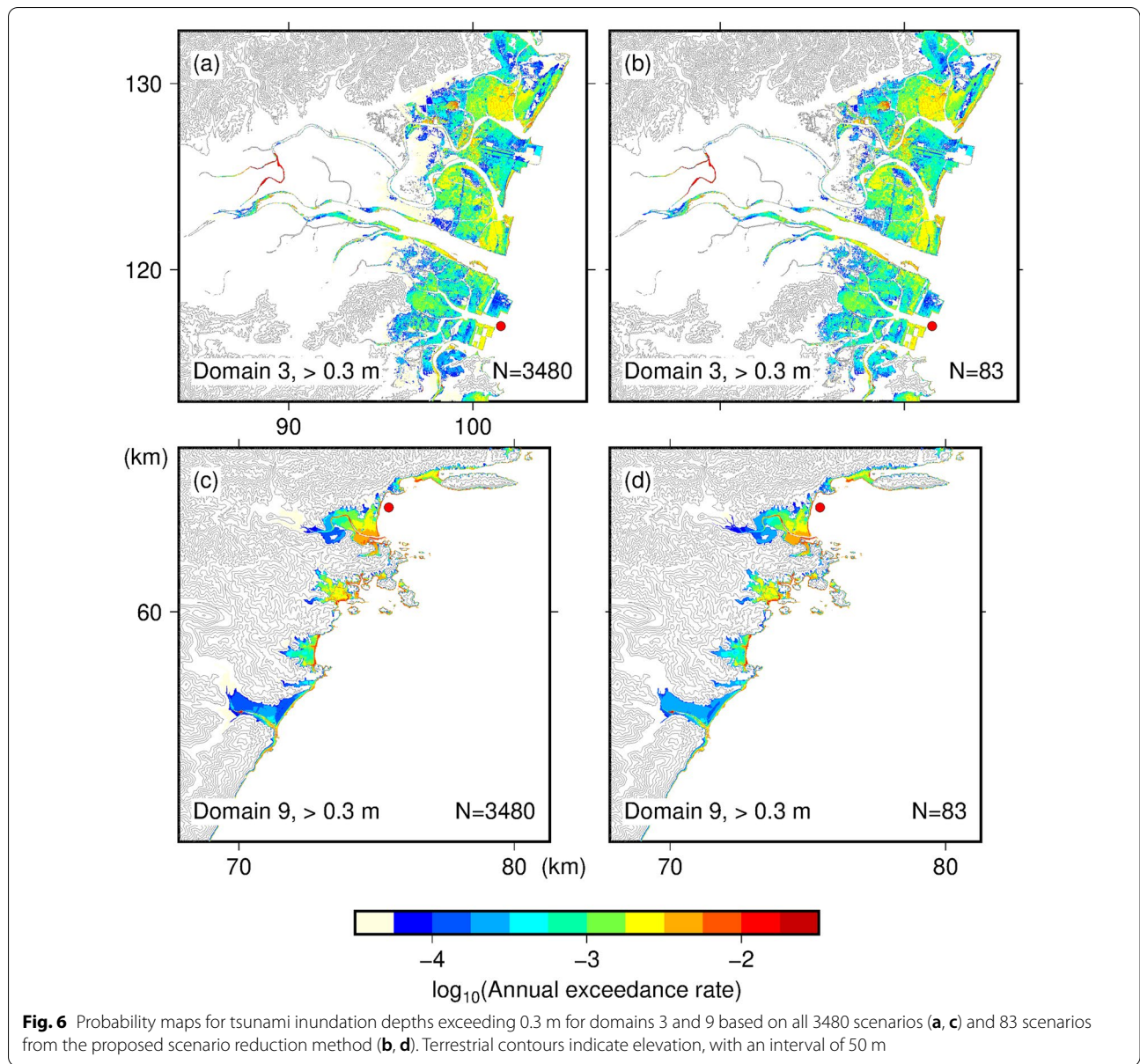We obtained historical tsunami data, which is the most reliable tsunami trace data in eastern Shikoku,

Baba *et al. Earth, Planets and Space* (2022) 74:156

Page 11 of 17

Fig. 5 Tsunami hazard curves estimated using heterogeneous slip models and tsunami defense facilities (red, original), homogeneous slip models and defense facilities (gray), and with heterogeneous slip models and no defense facilities (dashed blue) at 6 sites (Fig. 1). The black circles are the exceedance frequencies estimated from the historical tsunamis listed in Table 2, and the gray circles are those excluding the 1605 Keicho tsunami

from the study conducted by Murakami et al. (1996). We used the fault models of past earthquakes proposed by Annaka et al. (2003) (Table 2) to calculate the tsunamis that Murakami et al. (1996) did not report. Although more than half of the tsunami heights listed in Table 2 were not observed, but rather were calculated using the fault models of Annaka et al. (2003), these fault models adequately simulated the historical tsunami data presented by Murakami et al. (1996).

Therefore, we assumed that the fault models were reliable.

The oldest tsunami source model provided by Annaka et al. (2003) was for the 1498 Meio earthquake. In this study, we assumed the period from the 1498 Meio earthquake to right before the subsequent Nankai Trough earthquake, which could occur in the twenty-first century, to be 550 years. For example, the Tokushima tsunami height exceeded a meter four times and the

Baba *et al. Earth, Planets and Space*   (2022) 74:156

Page 12 of 17

Fig. 6 Probability maps for tsunami inundation depths exceeding 0.3 m for domains 3 and 9 based on all 3480 scenarios (**a**, **c**) and 83 scenarios from the proposed scenario reduction method (**b**, **d**). Terrestrial contours indicate elevation, with an interval of 50 m

Tachibana tsunami height seven times. Their annual rates were calculated to be $4/550 = 7.27 \times 10^{-3}$ and $7/550 = 1.27 \times 10^{-2}$ times/year, respectively. Similarly, we obtained the annual exceedance rates for historical tsunami heights of 3 and 5 m. If there was a range of observed tsunami heights in Table 2, we used a higher value. Figure 5 plots the annual exceedance rate of 1, 3, and 5 m at the 6 points with black circles on the hazard curves. The 1605 Keicho earthquake exhibited the features of a tsunami earthquake (Kanamori 1972) with almost no records of shaking damage, but there was an enormous tsunami. The source mechanism of earthquake is controversial. Harada et al. (2013) proposed that this

earthquake was not a Nankai Trough earthquake, but a giant interplate earthquake along the Izu-Ogasawara trench. The PTHAs in this study were only for interplate earthquakes occurring in the Nankai Trough. The tsunami from the other region should be excluded when calculating the annual exceedance frequency for comparison. Therefore, we calculated the annual exceedance rate without tsunami data from the 1605 Keicho earthquake (gray circles).

As shown in Fig. 5, the annual exceedance rate of historical tsunamis is consistent with the tsunami hazard curves without the tsunami defense facilities. Accordingly, we concluded that the proposed PTHA method
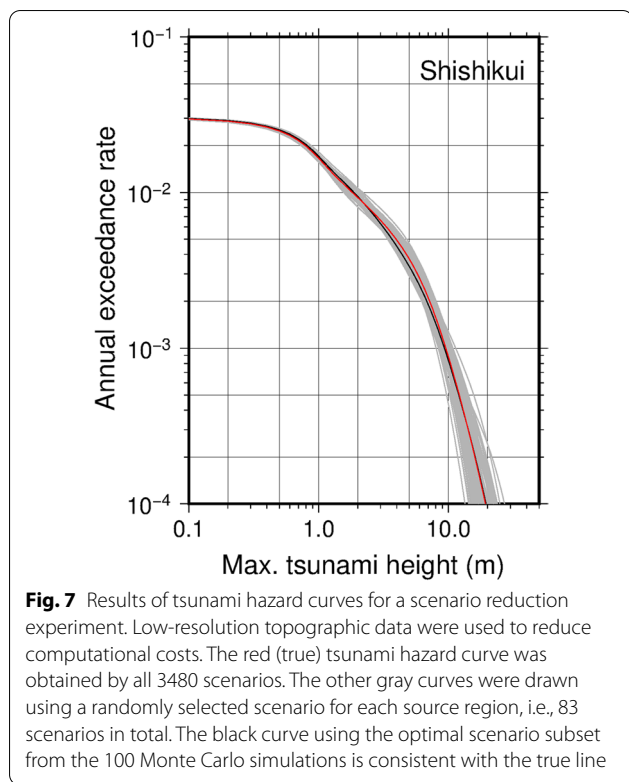
Fig. 7 Results of tsunami hazard curves for a scenario reduction experiment. Low-resolution topographic data were used to reduce computational costs. The red (true) tsunami hazard curve was obtained by all 3480 scenarios. The other gray curves were drawn using a randomly selected scenario for each source region, i.e., 83 scenarios in total. The black curve using the optimal scenario subset from the 100 Monte Carlo simulations is consistent with the true line

was appropriate. However, the exceedance rate at 1.0 m for the historical tsunamis was slightly lower than the estimated hazard curve, which indicates that we may have failed to observe tsunamis caused by medium-sized historical earthquakes.

Reducing scenarios

High-resolution tsunami calculations were performed using all 3480 heterogeneous slip models by high-performance computers. However, it is not always possible to use a high-performance computer, so reducing the number of tsunami calculation scenarios is desirable, particularly in PTHAs for tsunami inundation that require high-resolution calculation. We investigated a new

method for scenario reduction using random numbers. In this method, we computed all 3480 tsunami cases using a low-resolution topography model that excluded the 30 and 10 m grids from the original nested grid system of 810–270–90–30–10 m grids. The results obtained for 3480 low-resolution calculations show the tsunami hazard curves at the PTHA target area. Then, using the low-resolution results, the second step randomly selected one heterogeneous slip model from each source region to draw the tsunami hazard curves. In other words, we reduced the number of heterogeneous slip models from 3480 to 83, which is equivalent to the number of source regions. The tsunami hazard curve plotted using the selected 83 scenarios differed from the hazard curves derived from the 3480 cases. However, we repeated this procedure 100 times to determine a subset of 83 heterogeneous slip models, creating a curve that was almost identical to the 3480-case one. This procedure could reduce the number of scenarios while maintaining the shape of the hazard curve in front of the target area. Figure 7 shows the results of this experiment for Shishikui. Then, high-resolution tsunami calculations were performed for only the 83 cases selected as the optimal subset to construct the probabilistic tsunami inundation maps. We reduced the high-resolution tsunami calculations from 3480 to 83 cases.

Figure 6b, d shows the PTHAs of the obtained tsunami inundation depths for domains 3 and 9 using only the optimal subset of the high-resolution calculation results. These maps are consistent with the original PTHA maps (Fig. 6a, c) at rates exceeding $10^{-4.25}$ times/year corresponding to 17,000 years in the return period. We can conclude that the proposed method yielded the same results as the inundation probability distribution using all 3480 cases by using only 83 cases within a recurrence interval of approximately 10,000 years. Conversely, there is a discrepancy in the light-yellow area at a rate below $10^{-4.25}$ times/year (Fig. 6a, c). This discrepancy depends on whether the 83 selected scenarios included extensive

Table 2 Historical tsunami heights at the hazard curve points

St. name	Eq. name						
	1498 Meio	**1605 Keicho**	**1707 Hoei**	**1854 Tokai**	**1854 Nankai**	**1944 Tonankai**	**1946 Nankai**
Tokushima	*0.5*	*2.4*	*2.2*	*0.5*	**1–2**	*0.3*	**1.4**
Tachibana	*1.2*	*3.5*	**3–4**	*1.1*	**3**	*1.3*	**4.0**
Tai	*1.8*	*5.9*	*5.6*	*1.9*	**4.3**	*1.5*	**2**
Hiwasa	*1.0*	*4.9*	*4.5*	*1.0*	**2–3**	*0.8*	**2.5, 3.6**
Asakawa	*3.3*	**9**	**6–7**	*3.2*	**6.5–7.2**	*2.1*	**4.7–5.3**
Shishikui	*1.5*	**5–6**	*5.5*	*1.4*	**3.2–7.9**	*1.0*	**3.6**

Values in bold were obtained from Murakami et al. (1996). Values in italics were calculated using fault models proposed by Annaka et al. (2003). Units in meters

Table 3 Population in the expected tsunami inundation area (domain 3)

Conditions		Population	Ratio of total population (%)
Deterministic (maximum size)	ID > 0.3 m	296,686	70.8
	ID > 2.0 m	268,690	64.1
Probabilistic (this study)	P(ID > 0.3 m; 100 year) > 0.5	60,629	14.5
	P(ID > 2.0 m; 100 year) > 0.5	13,969	3.3

ID inundation depth

earthquake events. The extreme events included in the original set of all cases ($N = 3480$) need not be included in the selected subset of 83 cases reproducing the tsunami hazard curves. Therefore, we can assess tsunami risks for recurrence intervals below approximately 10,000 years using the PTHA maps derived from a small number of scenarios. The probabilistic hazard assessment of natural disasters usually can be limited to less than 10,000 years for practical use. When it is indispensable for hazards with a period exceeding 10,000 years, we suggest indicating low probabilities in the area between the inundation limits of the probability distribution and the extreme tsunami scenario.

A source region should contain multiple heterogeneous slip models, as slip heterogeneity impacts PTHAs (Fig. 5). In contrast, the total probability is calculated by multiplying the probability of earthquake occurrence with the exceedance probability of tsunamis for all scenarios (Eq. 3). Assuming that a set of heterogeneous slip models with a small number can be obtained to reproduce the total probability estimated using all of the heterogeneous slip models, the set of selected slip models should also reproduce the probabilistic maps of tsunami inundation. However, a similar approach cannot be valid for a set of homogeneous slip models with a large σ. This is because the procedure used in this study only defined the vertical variations in tsunami height. The maximum model of the selected slip models determined the horizontal limits of the tsunami inundation, which did not vary. Therefore, PTHAs obtained using a set of homogeneous slip models predicted tsunami inundation areas that were smaller than those obtained using all of the heterogeneous slip models.

Applications to practical problems

Urban planning for tsunami disaster prevention involves the use of a deterministic tsunami hazard map that indicates the expected tsunami inundation depth from an earthquake with a maximum magnitude. However, using the deterministic tsunami hazard map alone limits urban planning methods in areas where the expected tsunami is enormous. PTHA maps can provide opportunities to discuss alternative prevention measures and future urban structures in such areas. In domain 3, populated areas and infrastructure are located in areas with high tsunami hazards. Table 3 summarizes the relationship between tsunami hazard levels and populations from both deterministic and probabilistic points of view. The population data were obtained from the national census of Japan with the fourth-order mesh (500 m resolution), and calculations for 100-year exceedance probability used the homogeneous Poisson process. Because urban planning generally designs land use and social infrastructure with a target year several tens of years ahead, the 100-year exceedance probability is a reasonable period for future urban planning.

As shown in Table 3, the population of the area where the tsunami inundation depth is ≥ 0.3 m in the deterministic hazard map is 296,686, while the population of the area where the exceedance probability of inundation depth is ≥ 0.5 m is 60,629. The population was significantly decreased. Although tsunamis caused by the maximum-sized earthquakes induce tremendous tsunami inundation in all areas, probabilistic assessments considering various types of earthquakes revealed that several areas are prone to inundation, while others are not. We should improve the hardware that prevents tsunami disasters, such as breakwaters, seawalls, and evacuation lots. Because it is impossible to develop these measures simultaneously in all high risk areas, we must determine the construction order. PTHA maps can identify areas with a large population and high tsunami probability, thus prioritizing disaster measurements.

Conclusions

This study used the most reliable earthquake source scenarios proposed by Fujiwara et al. (2020), who investigated the characteristics of past interplate earthquakes in the Nankai Trough and other subduction zones. The utilization of high-performance computers enabled

high-resolution tsunami computations for all earthquake scenarios. The earthquake occurrence probability was based on the G-R law equation using an earthquake catalog for this region. The calculated tsunami heights included uncertainties using the variation index from Aida (1978). PTHAs were conducted for eastern Shikoku in the Nankai Trough, Japan. Based on the findings, the following conclusions were reached:

1. In the sensitivity analysis, a significant difference was observed between the hazard curves derived from the heterogeneous slip models and those from the homogeneous slip models. Therefore, PTHAs must include earthquake slip heterogeneity.
2. The effect of tsunami defense facilities was also observed in the hazard curves for Asakawa Bay. Therefore, PTHAs could support the construction of defense facilities from a cost–benefit standpoint.
3. The estimated tsunami hazard curves agreed with the frequencies of historical tsunamis. We therefore concluded that the PTHA procedure used herein is appropriate for estimating tsunami risks in the Nankai Trough.
4. We proposed a method for reducing tsunami computation loads for probabilistic tsunami inundation maps. This method successfully yielded probabilistic tsunami inundation maps similar to the original maps obtained using the complete method.

This study primarily aimed to compare the PTHA with the tsunami rates caused by the historical interplate earthquakes. We, therefore, performed the PTHAs for tsunamis caused by the interplate earthquakes only. For a comprehensive PTHA, it is necessary to include other tsunamis, such as intra-plate earthquake tsunamis, distant tsunamis, and non-seismic tsunamis. Because these tsunamis are probably smaller than those of the largest interplate earthquakes, the exceedance probabilities are expected to change in small and medium tsunami heights. The comprehensive PTHAs are challenging owing to the extensive research elucidating occurrence patterns and probabilities of intra-plate earthquakes, submarine landslides, volcanic eruptions, and meteorite impacts. However, these studies are essential to mitigating tsunami disasters. We intend to further investigate comprehensive PTHAs in the Nankai Trough.

Abbreviations
PTHA: Probabilistic tsunami hazard assessment; G-R law: Gutenberg–Richter law; JMA: Japan Meteorological Agency.

Supplementary Information
The online version contains supplementary material available at https://doi.org/10.1186/s40623-022-01715-1.

Additional file 1: Figure S1. Examples of the earthquake source scenarios. **Figure S2.** Probabilistic tsunami hazard assessment procedure. **Figure S3.** Tree structure for earthquake occurrence probability. **Figure S4.** Probability maps for tsunami inundation depths.

Author contributions
TB performed most of the tsunami simulations and probabilistic analysis, and wrote most of this manuscript. MK and RY calculated tsunami simulations on high-performance computers. NT and YS performed the sensitivity analysis. KW contributed to the discussion in "Applications to practical problems". HF constructed the heterogeneous slip models. All authors read and approved the final manuscript.

Availability of data and materials
The heterogeneous slip models can be downloaded at "J-THIS tsunami hazard station", https://www.j-this.bosai.go.jp/, last accessed on 10 June 2022. We used the tsunami software JAGURS (Baba et al. 2015, 2017) provided in an online repository at http://dx.doi.org/10.5281/zenodo.3737816. Owing to the large size of the tsunami calculation results, we do not upload them on online repositories. The readers can contact us directly for access to the data. The Japan tsunami trace database is at https://tsunami-db.irides.tohoku.ac.jp/tsunami/?LANG=-2, last accessed on 15 March 2021. The JMA earthquake catalog is available at https://www.data.jma.go.jp/svd/eqev/data/bulletin/hypo_e.html, last accessed on August 30, 2021. The JMA tide table is at https://www.data.jma.go.jp/gmd/kaiyou/db/tide/suisan/index.php, last accessed on September 1, 2021.

Declarations

Ethics approval and consent to participate
Not applicable.

Consent for publication
Not applicable.

Competing interests
The authors declare that they have no competing interests.

Author details
[1] Graduate School of Technology, Industrial and Social Sciences, Tokushima University, Tokushima, Japan. [2] Graduate School for Science and Technology for Innovation, Tokushima University, Tokushima, Japan. [3] Research Center for Management of Disaster and Environment, Tokushima University, Tokushima, Japan. [4] National Research Institute for Earth Science and Disaster Resilience, Tsukuba, Japan.

Baba *et al. Earth, Planets and Space*   (2022) 74:156

Page 16 of 17

References

Aida I (1978) Reliability of a tsunami source model derived from fault parameters. J Phys Earth 26(1):57–73. https://doi.org/10.4294/jpe1952.26.57

Anderson JG, Brune JN (1999) Probabilistic seismic hazard analysis without the ergodic assumption. Seismol Res Lett 70(1):19–28. https://doi.org/10.1785/gssrl.70.1.19

Annaka T, Inagaki K, Tanaka H, Yanagisawa K (2003) Characteristics of great earthquakes along the Nankai trough based on numerical tsunami simulations. J Earthq Symp 27:39. https://doi.org/10.1153/proee2003.27.39

Annaka T, Satake K, Sakakiyama T, Yanagisawa K, Shuto N (2007) Logic-tree approach for probabilistic tsunami hazard analysis and its applications to the Japanese coasts. Pure Appl Geophys 164:577–592. https://doi.org/10.1007/s00024-006-0174-3

Baba T, Takahashi N, Kaneda Y, Ando K, Matsuoka D, Kato T (2015) Parallel implementation of dispersive tsunami wave modeling with a nesting algorithm for the 2011 Tohoku tsunami. Pure Appl Geophys 172:3455–3472. https://doi.org/10.1007/s00024-015-1049-2

Baba T, Allgeyer S, Hossen J, Cummins PR, Tsushima H, Imai K, Yamashita Y, Kato T (2017) Accurate numerical simulation of the far-field tsunami caused by the 2011 Tohoku earthquake, including the effects of boussinesq dispersion, seawater density stratification, elastic loading, and gravitational potential change. Ocean Model 111:46–54. https://doi.org/10.1016/j.ocemod.2017.01.002

Behrens J, Løvholt F, Jalayer F, Lorito S et al (2021) Probabilistic Tsunami Hazard and Risk Analysis: A Review of Research Gaps. Front Earth Sci 9:628772. https://doi.org/10.3389/feart.2021.628772

Cabinet Office, Government of Japan (2012) Massive earthquake model review meeting of the Nankai trough. **(in Japanese)** http://www.bousai.go.jp/jishin/nankai/model/index.html. Accessed 20 Aug 2022

Cornell CA (1968) Engineering seismic risk analysis. Bull Seism Soc Am 58(5):1583–1606. https://doi.org/10.1785/BSSA0580051583

Crempien JGF, Urrutia A, Benavente R, Cienfuegos R (2020) Effects of earthquake spatial slip correlation on variability of tsunami potential energy and intensities. Sci Rep 10:8399. https://doi.org/10.1038/s41598-020-65412-3

Davies G, Horspool N, Miller V (2015) Tsunami inundation from heterogeneous earthquake slip distributions: evaluation of syn–thetic source models. J Geophys Res Solid Earth 120:6431–6451. https://doi.org/10.1002/2015JB012272

Fujiwara H, Hirata K, Nakamura H et al (2020) Probabilistic Tsunami hazard assessment for earthquakes occurring along the Nankai trough—volume 1 part I –. Tech Natl Res Ins Earth Sci Disaster Resil 439:71

Fukutani Y, Suppasri A, Imamura F (2015) Stochastic analysis and uncertainty assessment of tsunami wave height using a random source parameter model that targets a Tohoku-type earthquake fault. Stoch Environ Res Risk Assess 29:1763–1779. https://doi.org/10.1007/s00477-014-0966-4

Fukutani Y, Moriguchi S, Terada K, Otake Y (2021) Time-dependent probabilistic tsunami inundation assessment using mode decomposition to assess uncertainty for an earthquake scenario. J Geophys Res Oceans. https://doi.org/10.1029/2021JC017250

Furumura T, Imai K, Maeda T (2011) A revised tsunami source model for the 1707 Hoei earthquake and simulation of tsunami inundation of Ryujin Lake, Kyushu. Japan J Geophys Res Solid Earth 116:B02308. https://doi.org/10.1029/2010JB007918

Geist EL (2002) Complex earthquake rupture and local tsunamis. J Geophys Res. https://doi.org/10.1029/2000JB000139

Geist EL, Parsons T (2006) Probabilistic analysis of tsunami hazards. Nat Hazards 37:277–314. https://doi.org/10.1007/s11069-005-4646-z

Glimsdal S, Løvholt F, Harbitz CB et al (2019) A new approximate method for quantifying tsunami maximum inundation height probability. Pure Appl Geophys 176:3227–3246. https://doi.org/10.1007/s00024-019-02091-w

Goda K, Mai PM, Yasuda T, Mori N (2014) Sensitivity of tsunami wave profiles and inundation simulations to earthquake slip and fault geometry for the 2011 Tohoku earthquake. Earth Planet Sp 66:105. https://doi.org/10.1186/1880-5981-66-105

Gutenberg B, Richter CF (1941) Seismicity of the earth. Geological Society of America Special Papers, Boulder

Harada T, Ishibashi K, Satake K (2013) Tsunami numerical simulation for hypothetical giant or great earthquakes along the Izu-Bonin Trench. In: Abstract of American Geophysical Union fall meeting 2013:NH51A-1605. Headquarters for Earthquake Research Promotion (2013). Long-term evaluation of seismicity in the Nankai Trough (2nd Edition), 96

Hatori T (1978) Monuments of the Nankaido tsunamis of 1605, 1707 and 1854 in the Shikoku district: behavior of historical tsunamis and their comparison with the 1946 Nankaido tsunami. Bull Earth Res Inst 53:423–445

Hatori T (1981) Field investigation of the Nankaido tsunamis in 1707 and 1854 along the south-west cast of Shikoku. Bull Earth Res Inst 56:547–570

Hatori T (1988) Tsunami behaviors in the Seto inland sea and Bungo channel chase by the Nankaido earthquakes in 1707, 1854, and 1946. Zisin 1(41):215–221. https://doi.org/10.4294/zisin1948.41.2_215

Ishibashi K (2004) Status of historical seismology in Japan. Ann Geophys 47:339–368. https://doi.org/10.4401/ag-3305

Tohoku University's School of Engineering & the Japan Nuclear Energy Safety Organization (JNES), Japan tsunami trace database. https://tsunami-db.irides.tohoku.ac.jp/tsunami/?LANG=-2. last accessed on 15 March 2021.

Kajiura K (1963) The leading wave of a tsunami. Bull Earthquake Res Inst 41:535–571

Kanamori H (1972) Mechanism of tsunami earthquakes. Phys Earth Planet Inter 6:346–359. https://doi.org/10.1016/0031-9201(72)90058-1

Kitou T, Hirata K, Maeda T, Dohi Y, Fujiwara H, Matsuyama H (2021) Characterized fault models for the reproduction of the tsunami traces by the great earthquakes along the Nankai–trough towards probabilistic tsunami hazard assessment –. J Jap Asso Earth Eng. 21(1):1_82-1_105. https://doi.org/10.5610/jaee.21.1_82

Koshimura S, Namegaya Y, Yanagisawa H (2009) Tsunami fragility—a new measure to identify tsunami damage —. J Disaster Res 4(6):479–488. https://doi.org/10.2096/jdr.2009.p0479

Kotani T, Tazoto K, Takase S, Moriguchi S, Terada K, Fukutani Y, Otake Y, Nojima K, Sakuraba M, Choe Y (2020) Probabilistic tsunami hazard assessment with simulation-based response surfaces. Coast Eng 160:103719. https://doi.org/10.1016/j.coastaleng.2020.103719

LeVeque RJ, Waagan K, González FI, Rim D, Lin G (2016) Generating random earthquake events for probabilistic tsunami hazard assessment. In: Geist EL, Fritz HM, Rabinovich AB, Tanioka Y (eds) Global tsunami science past and future volume I. Springer, Cham

Lorito S, Selva J, Basili R, Romano F, Tiberti MM, Piatanesi A (2015) Probabilistic hazard for seismically induced tsunamis: accuracy and feasibility of inundation maps. Geophys J Inter 200(1):574–588. https://doi.org/10.1093/gji/ggu408

Løvholt F, Glimsdal S, Harbitz CB, Zamora N, Nadim F, Peduzzi P, Dao H, Smebye H (2012) Tsunami hazard and exposure on the global scale. Earth Sci Rev 110:58–73. https://doi.org/10.1016/j.earscirev.2011.10.002

Løvholt F, Griffin J, Salgado-Gálvez M (2015) Tsunami hazard and risk assessment on the global scale. In: Meyers R (ed) Encyclopedia of complexity and systems science. Springer, Berlin

Melgar D, LeVeque RJ, Dreger DS, Allen RM (2016) Kinematic rupture scenarios and synthetic displacement data: an example application to the cascadia subduction zone. J Geophys Res Solid Earth 121:6658–6674. https://doi.org/10.1002/2016JB013314

Mueller C, Power W, Fraser S, Wang X (2015) Effects of rupture complexity on local tsunami inundation: implications for probabilistic tsunami hazard assessment by example. J Geophys Res Solid Earth 120:488–502. https://doi.org/10.1002/2014JB011301

Mulia IE, Ishibe T, Satake K, Gusman AR, Murotani S (2020) Regional probabilistic tsunami hazard assessment associated with active faults along the eastern margin of the Sea of Japan. Earth Planet Sp 72:123. https://doi.org/10.1186/s40623-020-01256-5

Murakami H, Shimada T, Itoh S, Yamamoto N, Ishizuka J (1996) Reexamination of the height of the 1605, 1707 and 1854 Nankai tsunamis along the coast off Shikoku Island. J JSNDS 15(1):39–52

Obara K (2002) Nonvolcanic deep tremor associated with subduction in southwest Japan. Science 296:1679–1681. https://doi.org/10.1126/science.1070378

Obara K, Kato A (2016) Connecting slow earthquakes to huge earthquakes. Science 353:253–257. https://doi.org/10.1126/science.aaf1512

Obara K, Hirose H, Yamamizu F, Kasahara K (2004) Episodic slow slip events accompanied by non-volcanic tremors in southwest Japan subduction zone. Geophys Res Lett 31:L23602. https://doi.org/10.1029/2004GL020848

Okada Y (1985) Surface deformation due to shear and tensile faults in a half-space. Bull Seism Soc Am 75:1435–1154. https://doi.org/10.1785/BSSA0750041135

Tokushima Prefecture (2012) Tsunami hazard maps in Tokushima Prefecture. (**in Japanese**) https://anshin.pref.tokushima.jp/docs/2012121000010/. Accessed on 20 Aug 2022

Satake K, Fujii Y, Harada T, Namegaya Y (2013) Time and space distribution of coseismic slip of the 2011 tohoku earthquake as inferred from tsunami waveform. Bull Seism Soc Am 103:1473–1492. https://doi.org/10.1785/0120120122

Senior Seismic Hazard Analysis Committee (SSHAC). (1997) Recommendations for probabilistic Seismic hazard analysis: Guidance on uncertainty and use of experts. NUREG/CR-6372 UCRL-ID-122160 vol. 1, U.S. Nuclear Regulatory Commission. 256pp.

Sepúlveda I, Liu PL-F, Grigoriu M, Pritchard M (2017) Tsunami hazard assessments with consideration of uncertain earthquake slip distribution and location. J Geophys Res Solid Earth 122:7252–7271. https://doi.org/10.1002/2017JB014430

Shuto N (1993) Tsunami intensity and disasters. In: Tinti S (ed) Tsunamis in the world. Springer, Dordrecht

Tanioka Y, Satake K (1996) Tsunami generation by horizontal displacement of ocean bottom. Geophys Res Lett 23:861–864. https://doi.org/10.1029/96GL00736

Thio HK, Li W (2015) Probabilistic tsunami hazard analysis of the Cascadia subduction zone and the role of epistemic uncertainties and aleatory variability. the 11th Canadian conference on earthquake engineering, Canadian Asso Earthq Eng, 10

Toro GR, Abrahamson NA, Schneider JF (1997) Model of strong ground motions from earthquakes in central and eastern North America: best estimates and uncertainties. Seismol Res Lett 68(1):41–57. https://doi.org/10.1785/gssrl.68.1.41

Volpe M, Lorito S, Selva J, Tonini R, Romano F, Brizuela B (2019) From regional to local SPTHA: efficient computation of probabilistic tsunami inundation maps addressing near-field sources. Nat Hazards Earth Syst Sci 19:455–469. https://doi.org/10.5194/nhess-19-455-2019

Wessel P, Smith WHF, Scharroo R, Luis JF, Wobbe F (2013) Generic mapping tools: improved version released. EOS Trans Am Geophys Union 94(45):409–410. https://doi.org/10.1002/2013EO450001

Publisher's Note

Springer Nature remains neutral with regard to jurisdictional claims in published maps and institutional affiliations.